Available online at www.sciencedirect.com
ScienceDirect
Journal of the European Ceramic Society 30 (2010) 1105–1114
www.elsevier.com/locate/jeurceramsoc

The influence of pH on particle packing in YSZ coatings electrophoretically deposited from a non-aqueous suspension

Hui Xu, Ian P. Shapiro, Ping Xiao *

Manchester Materials Science Centre, University of Manchester, Manchester M1 7HS, UK

Available online 27 August 2009

Abstract

Yttria stabilized zirconia (YSZ) coatings were produced from a YSZ suspension in acetylacetone (ACAC) using electrophoretic deposition (EPD) and then sintered with substrate constraint at 1200 and 1300 °C. Before EPD, the operational pH of the suspension was adjusted by addition of acetic acid or triethanolamine (TEA) base. The effect of suspension pH on the deposition of EPD coatings was studied with respect to the suspension stability, coating density and microstructure. Results showed that the zeta potential had a high positive value on both sides of the iso-electric point (IEP). This probably resulted from the adsorption of TEA, detected by Fourier transform infrared spectroscopy. Three alkalies with different molecular structures were compared and the effect of their molecule length on the interparticle repulsion was discussed. Based on this, particle interactions were estimated for different pH suspensions. The reduced particle coagulation increased the packing density of the EPD coatings from 38% at pH 7.4 to 53% at pH 8.4. Therefore, subsequent sintering of coatings was promoted. The sinterability was evaluated by micro-hardness and microstructure. After sintering at 1200 °C, coatings made in pH 8.4 suspensions obtained a hardness of 786 MPa and had fewer big pores than coatings fabricated in pH 7.4 suspensions that had a hardness of 457 MPa.
© 2009 Elsevier Ltd. All rights reserved.

Keywords: Electrophoretic deposition (EPD); Porosity; Sintering; Microstructure; Hardness

1. Introduction

Electrophoretic deposition (EPD) is a colloidal processing technique which has been used to fabricate solid oxide fuel cells, micro-laminate and functionally graded materials, ceramic–matrix/ceramic–fibre composites[1] and porous layers as membranes[2] or thermal barrier coatings.[3] The process of EPD involves (1) particles acquiring surface charge in the suspension and moving towards one of the electrodes under the influence of the electric field; and (2) the charged particles forming a deposit on the surface of the electrode. The particle interaction is a critical factor to determine coating properties since it not only affect the particle migration during EPD via zeta potential, but also influences particle packing in the deposit via agglomeration. The subsequent processing of the deposits such as sintering is thereby influenced by the green coating properties as well.

When oxide powders are dispersed in polar solvents particles can develop a surface charge by desorbing of ions at the particle surface, chemical reaction at the solid–liquid interface or ions preferentially adsorbing onto the particle surface such as protons, metal ions or poly-electrolytes. Forces between neighbouring particles consist of intrinsic Van der Waals attraction and electrostatic repulsion due to the particle surface charge. In some systems other effects may also exist such as a steric force induced from the presence of surfactants or polymers, a structural force from the molecules of solution or a hydrophobic force from the hydrophobic surfaces of solids, etc.[4] According to the Darjaguin, Laundau, Verway and Overbeek (DLVO) theory, the stability of a colloid depends on the balance of all forces and the total potential energy of particle interactions.[5] Therefore, in order to obtain a stable colloid, a high surface charge/zeta potential is required to induce a high repulsive force.

The acidity of suspension as indicated by the pH value can influence the particle surface charge, which is indirectly measured by measurements of zeta potential. For an aqueous YSZ suspension, the suspension zeta potential is positive for low pH values and negative when pH increases above 4–6 (the iso-electric point, IEP).[6–9] For ethanol-based oxide suspensions, a similar relationship between the zeta potential and the pH is also observed.[10–12] Other work has also investigated the effect of acidity or the size of organic bases on the suspension properties.[13–15] However, due to the relatively low degree of

* Corresponding author. Tel.: +44 1613065941; fax: +44 1613063586.
E-mail address: ping.xiao@manchester.ac.uk (P. Xiao).

0955-2219/$ – see front matter © 2009 Elsevier Ltd. All rights reserved.
doi:10.1016/j.jeurceramsoc.2009.07.021

electrolyte dissociation in organic media, the ionic strength is reduced which greatly reduces the repulsive force between particles. In non-aqueous systems the potential determining ions may consist of a variety of species formed by either equilibrium ionization in the bulk solvent or by solid/liquid interfacial reactions.[16] These factors further complicate colloidal characterization for non-aqueous suspensions and the interrelationship between conductivity, zeta potential and pH needs to be further understood. The control of these factors is expected to be helpful in adjusting the particle interactions and consequently the green structure.

Since pH has a critical impact on the particle zeta potential, it has attracted great attention when the EPD process is studied. Sarkar and Nicholson[17] analysed the relationship between the interparticle interaction energy and stability ratio as a function of pH for an alumina–ethanol suspension and their experiments showed that the suspension had the lowest stability ratio around the IEP. Anne et al.[18] studied the influence of pH on the suspension resistivity, EPD yield and the particle double layer thickness of the same system. They found that the pH affected the potential drop across the suspension by changing the ionic strength. Fukada et al.[19] summarised IEP, mobility and stability properties with respect to pH for several oxides in ethanol suspensions. In general, pH was widely used as a path to evaluate the charging of particles by modifying zeta potential and thereby the suspension stability so that desirable deposits could be obtained. By this method, Chen et al.[2] successfully fabricated alumina membranes with tailored pore size distribution from ethanol suspension by EPD at low pH. They noticed that negligible deposition could be obtained around the IEP and worse deposition at higher pH due to stronger particle agglomeration. Ma et al.[20] suggested that there exists an optimum range of pH for a well dispersed PZT–ethanol suspension that produces a high green density after EPD. Tabellion and Clasen[21] reported that by the adjustment of pH in a B_4C–SiC–C aqueous suspension, a dense composite coating with carbon homogeneously dispersed can be deposited and well sintered. Santillan et al.[22] used HNO_3 and NaOH together with iodine to adjust nano-TiO_2 particles in ACAC suspension and stated that lowest viscosity can be obtained at around pH 5. Based on this, good coatings were fabricated at low EPD voltage. Most of these studies about pH were performed on aqueous or ethanol-based suspensions. More work is expected to be done on other non-aqueous systems especially on the effect of pH on the coating microstructure after EPD.

In order to develop the application of EPD coatings to thermal barrier coatings, the sintering must be undertaken at the relatively low temperature dictated by the metal substrate whilst retaining a certain degree of porosity. Besides improving green density, the reduction of agglomerate size of ceramic powders can also promote initial-stage sintering.[23,24] Thus, it is expected that by means of controlling the agglomeration of particles in the suspension, the sinterability of EPD coatings can be improved to some extent.

In this work, non-aqueous suspensions of yttria stabilized zirconia (YSZ) in acetylacetone (ACAC) with various pH are used to fabricate coatings by EPD. The colloidal properties of the suspensions and the coating microstructure and properties are studied. The effect of pH on particle packing during EPD and on sintering is also considered. The effects of alkalies with different molecular chain lengths on particle interactions are also compared.

2. Experimental procedure

2.1. Suspension preparation

The suspension was prepared by mixing 8 wt.% yttria stablized zirconia (YSZ, MELox5Y, 99.9%, tetragonal phase, MEL Chemicals, UK) in acetylacetone (ACAC, >99%, Sigma–Aldrich, UK) solvent with a solid content of 25 g/l. Ultrasonic agitation was applied to help disperse powder and reduce agglomeration. The pH of suspensions was adjusted between 4.4 and 8.4 through the addition of acetic acid (HAc) or triethanolamine (TEA), which is the maximum range of pH values possible since HAc and TEA are a weak acid and a weak alkali, respectively. The suspension conductivities were kept constant by adding a suitable amount of ammonium acetate salt ($NH_4C_2H_3O_2$) in order to exclude the influence of ionic strength changes on the particle interactions. The suspension concentration and the amount of additives are given in Table 1.

2.2. Characterization of colloidal properties

The pH and conductivity of suspensions were measured using a glass electrode pH meter (pH212, Hanna instruments, Italy) and conductivity meter (SevenMulti, Mettler Toledo, Switzerland), respectively. The pH value displayed by the meter (operational pH) differs from the real pH (negative logarithm of the proton activity in ACAC) due to the difference in partial Gibbs energy of H^+ atoms in water and ACAC, known as the medium effect.[25] For convenience, the pH value used in this study is the operational pH once prepared.

The particle size distribution was measured in freshly prepared suspension by laser scattering (Mastersizer, Micro Trac X100, Malvern, UK) and the particle zeta potential was estimated from the electrophoretic mobility measured using the

Table 1
Composition and properties of YSZ–ACAC suspensions.

pH	YSZ content (g/l)	Acid/alkali volume fraction	Conductivity (μs/cm)	Salt ($NH_4C_2H_3O_2$) concentration (g/l)
4.4	25	1.25% HAc	5	1.25
5.6	25	0.5% HAc	5	1.3
7.4	25	0	5	2.34
7.8	25	0.0125% TEA	5	1.56
8.4	25	0.625% TEA	5	0

Table 2
Molecular structure and concentration of the bases studied.

Alkali	Molecule structure	Approximated molecular length (nm)[a]	pH	Conductivity (μs/cm)	Alkali concentration
MEA	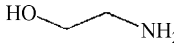	0.83	7.8	5	2.5%
TEA	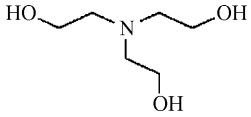	1.24	7.8	5	0.05%
AH		1.44	7.8	5	2.5 g/l

[a] The molecular chain length is estimated according to bond length.[7]

Electrokinetic Sonic Amplitude method (ESA-9800, Matec, USA). The suspension stability was evaluated by the Relative Sedimentation Height (R.S.H) method over 200 h. Fourier transform infrared spectroscopy (FT-IR; Nicolet 5700, Thermo Electron, USA) was employed to detect the chemical compounds adsorbed at the surface of particles from the EPD suspension.

2.3. EPD of coatings

Coatings were horizontally deposited on Fecralloy™ substrates (Fe72.6/Cr22.0/Al4.8/Si0.3/Y0.3 (wt.%), Goodfellow, UK). The advantages with use of the Fecralloy substrate are (1) Fecralloy is resistant to high temperature oxidation due to formation of alumina scale at surface of the substrate; (2) Fecralloy has a similar coefficient of thermal expansion with that of the YSZ coating ($11 \times 10^{-6}\,K^{-1}$)[26], which leads to low thermal mismatch between the coating and substrate; (3) Fecralloy is a high temperature alloy. With application of YSZ coatings, Fecralloy can be used in even harsher environment. EPD was carried out in freshly prepared suspensions at a constant electric field of $60\,V\,cm^{-1}$. The deposition time was adjusted between 30 s and 2 min to make crack-free coatings around 50 μm thick after ambient drying. The wet coating density was calculated from the mass immediately after EPD and that after the solvent had evaporated. The density of the green coating was calculated from the coating mass and dimensions for which the green coating thickness was obtained by the focal position change between the surface of the coating and the substrate using an optical microscope.

Isothermal sintering of the coating whilst under substrate constraint was carried out in ambient air for 6 h at 1200 and 1300 °C without cracking or delamination. The mercury intrusion method (Poremaster, Quantachrome, USA) was used to measure the porosity in the coating. Instrumented microhardness measurements (CSM Instruments, Switzerland) were made on the top surface of sintered samples with a loading of 0.2 or 0.3N (30 s loading, 10 s hold) to obtain the indentation hardness (H_{IT}) and Young's modulus values through the indentation depth. The microstructure of coatings after sintering was examined by scanning electron microscopy (SEM, XL30 FEG, Philips, Netherlands) on fracture surfaces and polished cross sections of the coatings.

In order to study the influence of surface adsorbed chemicals on the sintering of coatings, powders dried from various pH suspensions were ground and cold pressed into pellets with a relative green density of 50%. The pellets were sintered in air for 6 h at 1200 and 1300 °C. The density of the sintered pellets was measured by Archimedes' method in distilled water. Microhardness was measured on polished surfaces as described above.

In order to investigate the influence of the alkali molecular structure on the particle interactions, three weak bases, TEA, monoethanolamine (MEA) and 6-amino-1-hexanol (AH), with the same (hydroxyl and ammonium) chemical groups but with different molecular structures, were used to prepare suspensions. pH values of suspensions were adjusted to 7.8 and the concentration of each alkalies is listed in Table 2. Zeta potential and particle size distribution were compared for suspensions with different alkalies.

3. Results

3.1. Colloidal properties at various pH

Fig. 1 shows that the YSZ powder consisted of roughly spherical particles with a monodistributed primary size of around 0.26 μm. The particle size distributions in suspension (Fig. 2) show peaks around 6 μm across the pH range which probably result from the hard agglomeration of dry powders that cannot be broken up by the ultrasonic agitation. At pH 4.4 and 8.4 the mean sizes were around 0.3 μm which suggests that a portion of particles was well dispersed in the suspension and only

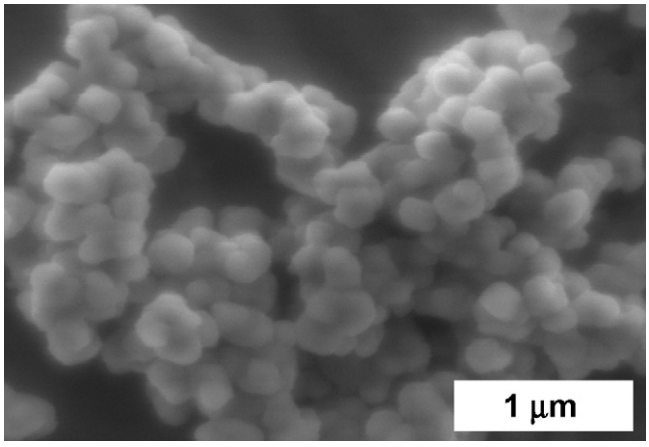

Fig. 1. Secondary electron SEM image of YSZ particles.

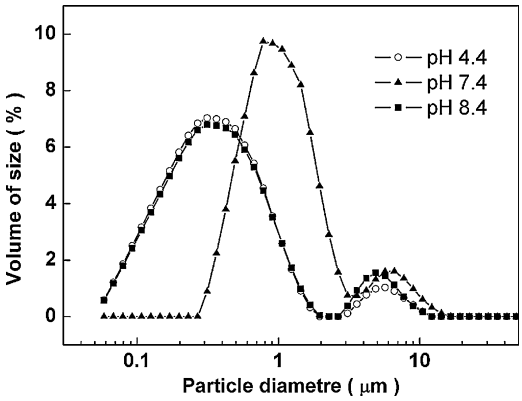

Fig. 2. Particle size distribution for suspensions at various pH.

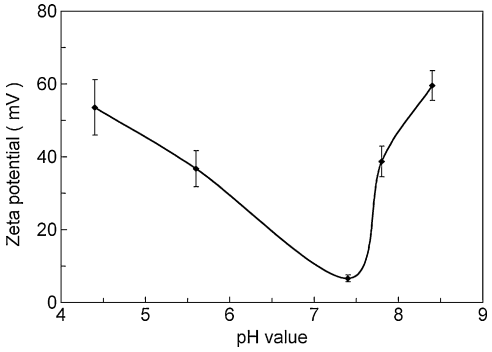

Fig. 3. Zeta potential as a function of suspension pH.

slight agglomeration occurred. At pH 7.4 particles displayed an agglomeration peak around 1 μm indicating that the particles were able to form big aggregates or networks in the suspension at this pH.

The zeta potential (ζ) of particles was always positive in the pH range studied here (Fig. 3). When the pH increased from 4.4 to 7.4, the zeta potential decreased and reached almost zero at pH 7.4 which is considered to be the iso-electric point (IEP) of this YSZ powder in ACAC. With pH increased further to 8.4, the zeta potential of particles increased and reached the maximum value of around +60 mV. This 'U'-shape ζ–pH relationship differs to that widely observed for aqueous suspensions. This suggests

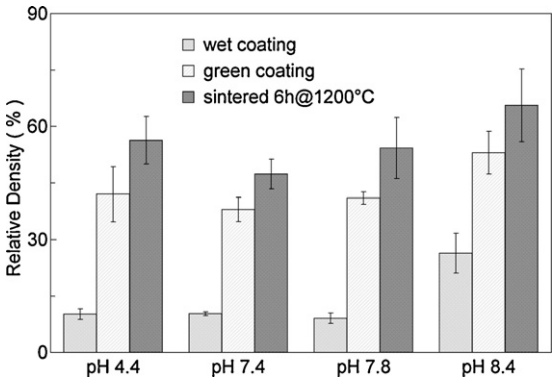

Fig. 5. Density of coatings after EPD, drying and sintering at 1200 °C for 6 h.

that the suspension can be stable at either pH 4.4 or 8.4 which agrees well with the relative sedimentation height measurements in Fig. 4. Fig. 4a shows that particles in pH 4.4 and 8.4 suspensions took approximatly 200 h to fully sediment and formed a layer of dense sediment at the bottom of the cylinders (Fig. 4b). For the pH 7.4 suspension, particles sedimented within in a few minutes and produced a thick layer which indicates that particles were loosely packed in the sediment. This is consistent with the flocculation of particles into a loose network around the IEP.

3.2. Coating properties after EPD and sintering

Coatings were fabricated by EPD from each suspension and the density was measured after drying and sintering. The results shown in Fig. 5 indicate that compared with other coatings, the pH 8.4 coatings showed the densest particle packing in both the wet deposit and green state as well as after sintering for 6 h at 1200 °C. Although starting with similar wet density to that made at pH 4.4, coatings made at pH 7.4 did not consolidate effectively during drying and sintering and resulted in a relatively low final density.

Pores were categorised into those with size less than and greater than 1 μm, described as micro- and macropores, respectively, which is schematically demonstrated in Fig. 6a. The porosity distribution in Fig. 6b suggests that coatings fabricated at different pH have a similar portion of micropores; however

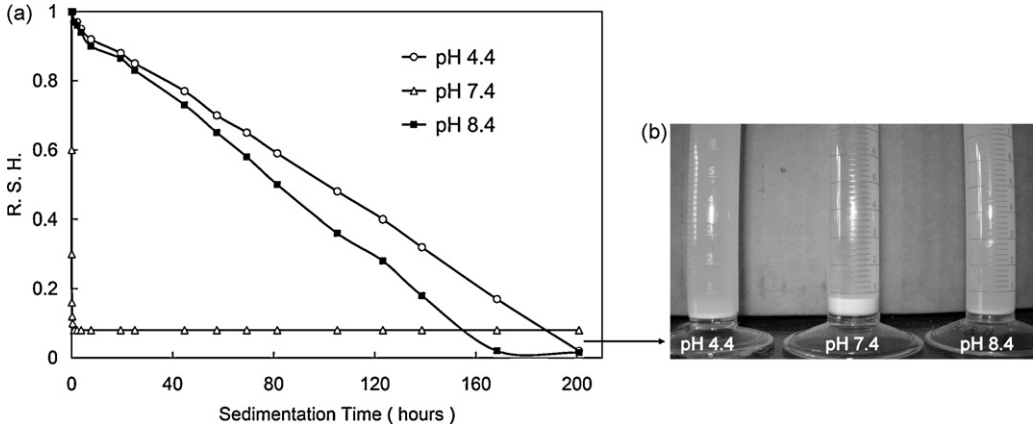

Fig. 4. Relative sedimentation height (R.S.H.) as a function of sedimentation time (a) and the suspensions after 200 h sedimentation (b).

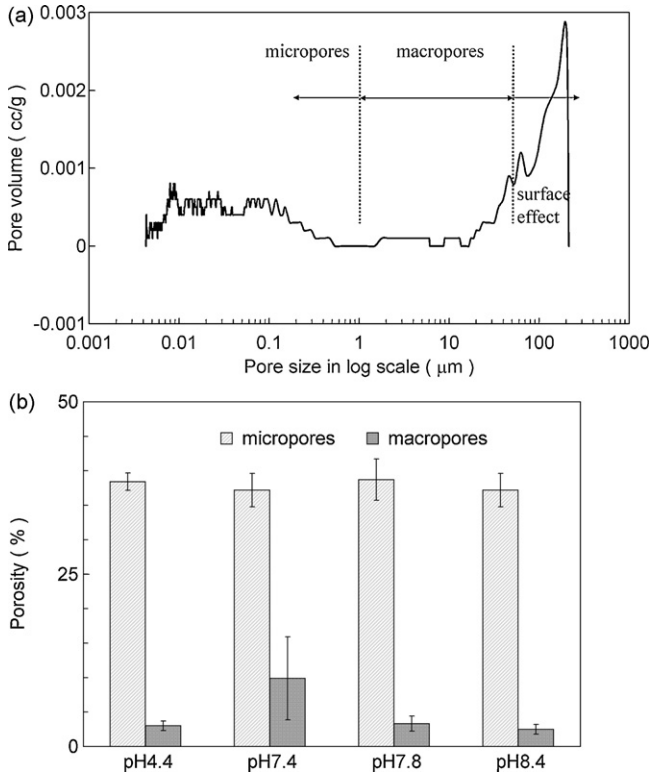

Fig. 6. Schematic of categorised pores according to their size (a) and proportion of porosity (b).

the macroporosity varies greatly. pH 7.4 coatings retained as much as a 10% volume of macropores after sintering, whilst coatings made at pH 4.4 and 8.4 showed the smallest portion of macropores, 3% and 2.5%, respectively.

Fig. 7 shows SEM images of sintered coatings where the pH 7.4 coating reveals several interconnected voids between networks of agglomerates which did not consolidate during sintering. Conversely the coatings made at pH 4.4 and 8.4 had fewer interconnected voids and hence achieved a higher hardness and density after sintering.

As the green coatings had minimal cohesion and hardness, the hardness of coatings after sintering is employed to evaluate the sinterability. In Fig. 8 the micro-hardness and Young's modulus results agree well with the trend in density with respect to pH. The denser the coating is after EPD the harder and stiffer the coating is after sintering. The properties of 1200 °C sintered coatings are most relevant here since it is considered that the low temperature sintering is dominated by the coating green microstructure which is the focus of this work. Plus, 1300 °C is too high for the alloys typically coated with TBCs.

3.3. Particle surface chemistry

The FT-IR spectra in Fig. 9 shows the chemical compounds adsorbed on the particle surface. Besides the inevitably adsorbed H_2O and CO_2, the –C=O group was detected in the pH 4.4 and 7.4 powders. This group may result from $Zr(ACAC)_4$ generated from the reaction of YSZ and ACAC, the anion (CH_3COO^-) of acetic acid or the salt ammonium acetate. Besides peaks corresponding to the spectra of TEA, the powder from pH 8.4 suspensions exhibited a peak at 1580 cm^{-1} that suggests the existence of secondary N–H bonds and an intensified peak around 3300 cm^{-1} which suggests the existence of either primary N–H bonds or intermolecular H–H bonds. This chemical compound was probably adsorbed on the YSZ surface and thus affected the particle interactions as well as their aggregation. According to sintering kinetics, impurities in the green body might affect surface diffusion and hence the sintering process. To clarify the effect of surface chemistry on sintering,[27] green pellets fabricated by cold pressing with the same density but different particle surface adsorptions were sintered. Table 3 indicates that starting from the same relative green density pellets made from powders with different surface adsorptions have similar density after sintering. Similarly no significant difference was measured between hardness of pellets sintered at 1200 and 1300 °C, actually the pH 8.4 sample showed around 11% lower hardness than the other two, which suggests that surface chemistry of this sample at least does not promote sintering. Thus, it is thought that although different chemicals were adsorbed onto the particle surface the sintering of the green body was not significantly affected.

3.4. Effect of alkali molecular structure on coating properties

As shown in Table 2 three alkalies with the same chemical groups but different molecular structure or length were used. Fig. 10 shows their effect on YSZ agglomerate size. The particle size distributions show a degree of agglomeration around 0.5–0.6 μm for all three alkalies, however compared with MEA and TEA, particles in suspensions with AH added seem less likely to form big coagulations of around 5 μm size. This agrees with the zeta potential measurements of the three suspensions. Fig. 11 shows that particles had similar magnitude of zeta potential in suspensions with MEA and TEA addition, however particles in suspension with AH added had a significantly higher zeta potential than the other two. This suggests that AH has a stronger ability to prevent the particle agglomeration, probably as it is a longer molecular chain.

4. Discussion

4.1. Charging mechanism for YSZ in ACAC

In a colloid with YSZ dispersed in ACAC, the dipole of the –OH group on the YSZ surface tends to capture protons from ACAC to form a positive charge on the particle surface, as shown by Eq. (1).[28] Moreover, the chemical reaction between YSZ and ACAC (Eq. (2)) is also thought to release a large number of protons.[29] Both of them help to create a positive zeta potential for particles.

$$(Zr{-}OH)_{surface} + CH_3COCH_2COCH_3 \rightarrow (Zr{-}OH_2)^+{}_{surface} + (CH_3CO)_2CH^- \quad (1)$$

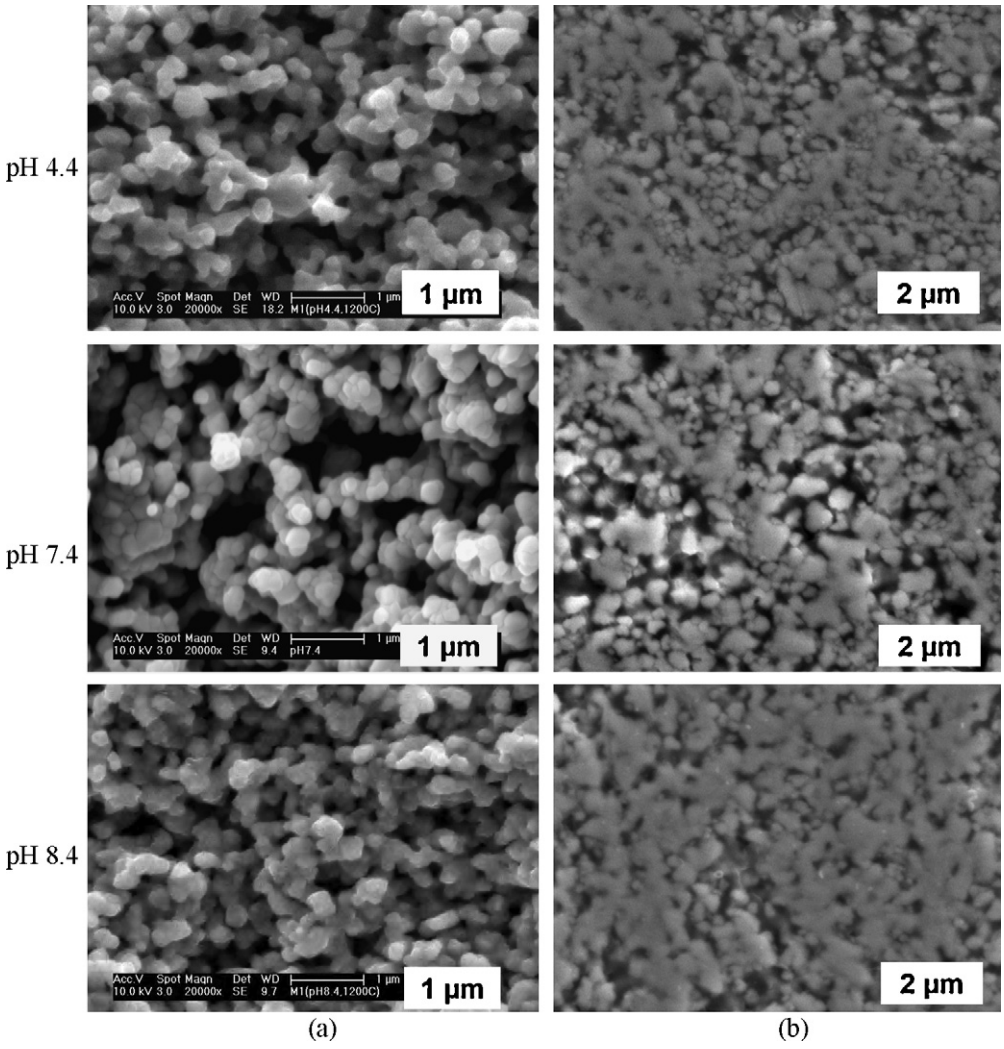

Fig. 7. Secondary electron SEM images of fractured (a) and polished (b) coatings made at different suspension pH after sintering at 1200 °C for 6 h.

$$Z_rO_2 + 4ACAC \rightarrow Z_r(ACAC)_4 + 2H^+ + 2OH \quad (2)$$

With the addition of acetic acid into the suspension, the particle zeta potential is increased through further adsorption of protons ionized by the acid. With the addition of TEA into the suspension, due to the lone pair of electrons on the nitrogen atom of TEA, it tends to capture H^+ from ACAC and form compounds $NH^+(CH_2CH_2OH)_3$ or $NH_2^{2+}(CH_2CH_2OH)_3$ (Eq. (3)) whose N–H bond appears on FT-IR spectra (Fig. 9). These compounds may tend to adsorb to YSZ particle surfaces (Fig. 14), which may also enrich the particle surface charge and account for the high positive zeta potential in pH 8.4 suspensions. Thus, in this experiment, the addition of either organic acid or alkali both promoted positive zeta potentials resulting in the 'U'-shape trend of the ζ–pH relationship.

$$N(–R–OH)_3 + ACAC \rightarrow HN^+(–R–OH)_3 + ACAC^- \quad (3)$$

4.2. Particle interactions in the suspensions

The relationship between pH and zeta potential was not as is commonly expected for aqueous systems, with YSZ in ACAC having positive zeta potential at both acid and alkali pH. However the influence of the magnitude of zeta potential on suspension stability was as expected with greater zeta potential providing a more stable suspension (Fig. 4).

Table 3
Properties of pellets made by powders with different chemicals adsorptions.

pH	Relative green density (%)	Sintered 6 h at 1200 °C		Sintered 6 h at 1300 °C	
		Density (%)	Hardness (MPa)	Density (%)	Hardness (MPa)
4.4	50	53.1 ± 2.3	1331.2 ± 342.0	87.7 ± 1.1	14897.8 ± 4302.7
7.4	50	54.2 ± 1.1	1358.5 ± 370.2	88.4 ± 1.9	12780.2 ± 1400.4
8.4	50	54.1 ± 1.5	1209.3 ± 262.2	86.2 ± 3.4	11539.4 ± 3093.2

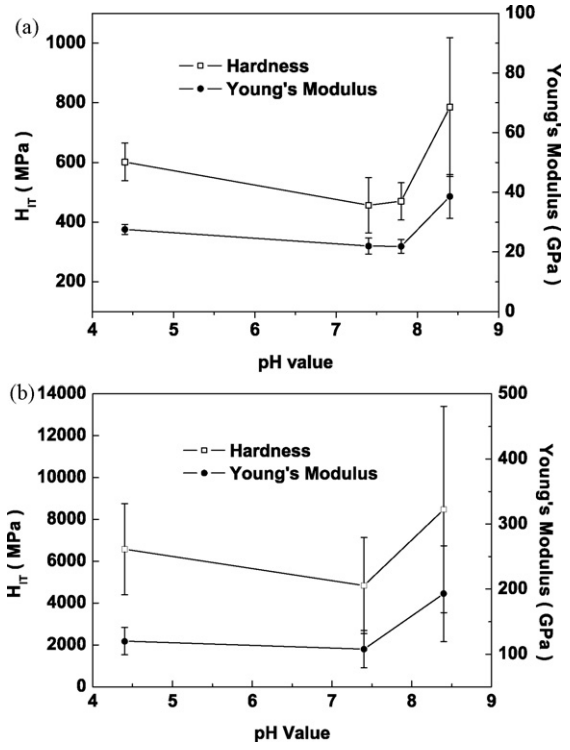

Fig. 8. Micro-hardness and Young's modulus of coatings sintered for 6 h at 1200 °C (a) and 1300 °C (b) for 6 h.

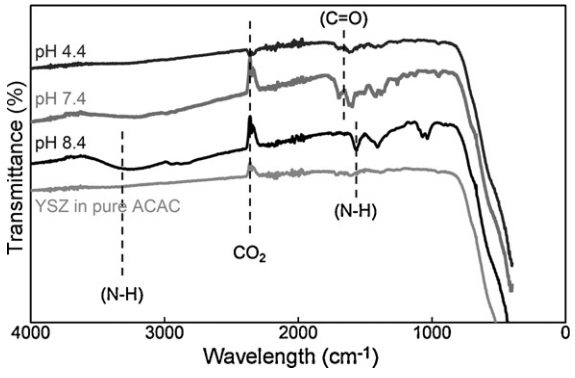

Fig. 9. FT-IR spectra of vacuum filtered powder showing chemical compounds adsorbed to the particle surfaces.

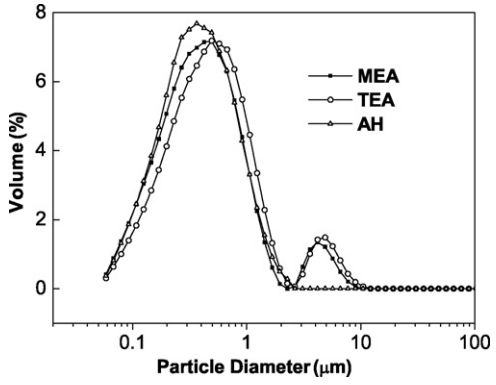

Fig. 10. Particle size distributions for suspensions with different alkali additions.

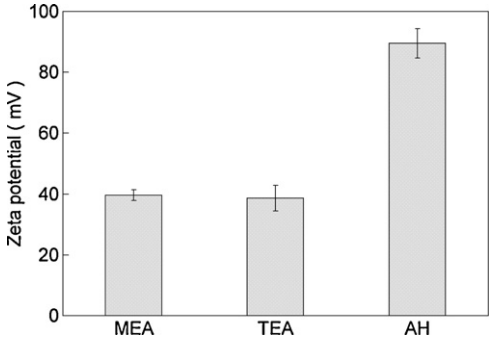

Fig. 11. Zeta potential of pH 7.8 suspensions with different alkali additives.

Since the zeta potential increased dramatically with the addition of AH compared to MEA and TEA (Fig. 11), it is thought that whilst the adsorption of all three alkalies contribute to the particle surface charge in the same way (Fig. 12), AH induced an extra steric effect due to its greater chain length.[14] Hence, it is hypothesised that in the TEA suspension, the shear plane is positioned between the molecule lengths of TEA and AH, which is approximately 1.4 nm from the particle surface (Fig. 13).[15] To simplify the calculation of particle interactions it is assumed that ions have similar mobility in the suspension, so that the different pH suspensions (with identical conductivity) will have similar ionic strengths and, according to Eq. (4), similar double layer thickness κ^{-1}. According to the DLVO theory, the potential energy of the electrostatic repulsion V_R can be obtained through Eq. (5) when $a\kappa > 10$,[30] in which the hypothetical thickness of double layer (1.4 nm) was used.[31]

$$\kappa^{-1} = \sqrt{\frac{\varepsilon_0 \varepsilon KT}{2nz^2e^2}} \tag{4}$$

$$V_R = -2\pi\varepsilon_0\varepsilon a\psi_0^2 In[1 - \exp(-\kappa H)] \tag{5}$$

where κ is the Debye–Huckel parameter (reciprocal of double layer thickness), ε_0 is the permittivity of a vacuum (8.85×10^{-12} F m^{-1}),[14] ε is the relative permittivity of the medium (26.5 for ACAC[32]), Z is the valence of the electrolyte, n is the ionic concentration, K is the Boltzmann constant, T is the absolute temperature, a is the particle radius (130 nm), H is the separation distance between particles and ψ_0 is the particle

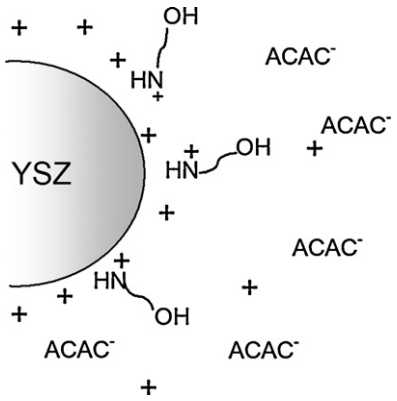

Fig. 12. Schematic of adsorbed TEA compounds.

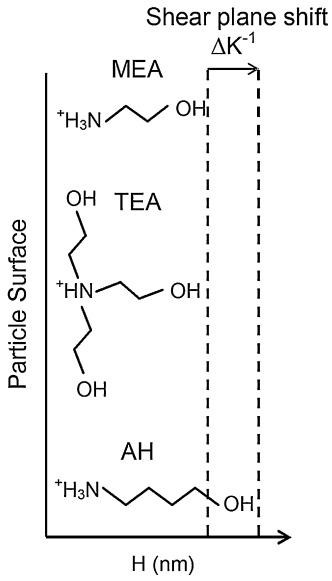

Fig. 13. Schematic of the possible double layer position with respect with different adsorbed alkali chain lengths.

surface potential which is assumed to be equal to particle zeta potential ζ.

The Van der Waals attraction energy and the calculation of Hamaker constant is given by[7,33]

$$V_A(H) = -\frac{(\sqrt{A_1} - \sqrt{A_2})^2 a}{12H} \quad (6)$$

$$A = \frac{3}{4}kT\frac{(\varepsilon-1)^2}{(\varepsilon+2)^2} + \frac{3h\upsilon_e(\alpha^2-1)^2}{16\sqrt{2}(\alpha^2+1)^{3/2}} \quad (7)$$

where A_1 and A_2 are the Hamaker constants of the particle and medium, respectively, which can be estimated by Eq. (7), ν_e is the main electronic adsorption frequency (typically around 3×10^{15} S^{-1})[33], h is Planck's constant and α is the refractive index (2.02 and 1.45 for YSZ[34] and ACAC[32], respectively). According to Eq. (7), values of 20.9×10^{-20} and 6.2×10^{-20} J for A_1 and A_2 can be estimated, respectively.

The total potential energy of interaction between two particles V_T can then be calculated as below and plotted in Fig. 14:[20]

$$V_T = V_A + V_R \quad (8)$$

The interaction energy curve (Fig. 14) indicates that for both the pH 4.4 and 8.4 suspensions there is increasing interparticle repulsion at closer than 1 nm separation that creates a potential energy

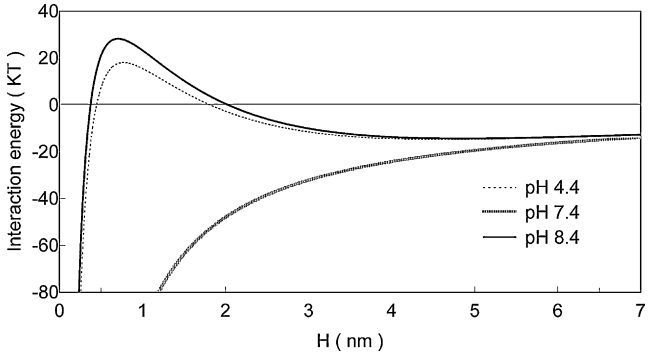

Fig. 14. Estimated total interaction energy (V_T) for suspensions with various pH.

barrier to the intrinsic van der Waals attraction and prevents the particle coagulation. Since the thermal energy of the particles (~10 kT[7]) is less than the potential maximum (~18 and ~28 kT) for these suspensions, coagulation should not occur. However, the gap between the thermal energy and the barrier is small. This can explain why these two suspensions were relatively stable but still able to form a moderate degree of agglomeration. For the suspension with pH at 7.4, the potential barrier disappears. This suggests that particles in this suspension are likely to coagulate which agrees with the particle size measurement and the sedimentation results. Thus, the particle surface charge has an important effect on particle agglomeration by tuning particle interactions.

4.3. The effect of microstructure on EPD and the sintering of coatings

The agglomeration of particles in suspension subsequently affects their packing in the coating. During EPD, the charged particles migrate toward the cathode in agglomerate 'blocks' under the electric field. Thus, similar to the video game Tetris, the deposition is the process of packing of the agglomerates. Smaller sized agglomerates are more likely to pack tightly than irregularly shaped particle networks. This effect is also seen in the final sediment height in Fig. 4. Moreover, it is considered that the zeta potential not only determines the mobility of particles in suspension but also the rearrangement of deposited particles during EPD.[28] At pH 4.4 or 8.4, the aggregates in the deposit can rearrange under the electric field to provide further densification; whilst due to the low zeta potential, particles in pH 7.4 suspensions are less able to move once they have

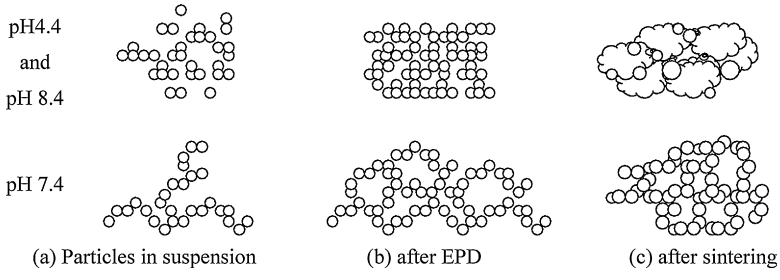

Fig. 15. Schematic of particle agglomeration structures and their effect on coating structure.

deposited and retain their loose packing after EPD and drying (Fig. 15).

The packing density of EPD coatings affects the subsequent sintering process and the final microstructure. Denser packing and a narrow pore size distribution give rise to more contact points between particles which are beneficial for sintering. According to Kellett and Lange,[35] small pores which normally have fewer contiguous particles surrounding them disappear in preference to large pores. Thus, after sintering at a temperature too low for complete sintering, coatings made at pH 4.4 and 8.4 sintered better, especially inside the agglomerates. For the coatings fabricated at pH 7.4, due to the loose particle interconnection, a greater number of big voids remained after sintering.

5. Conclusions

The adjustment of pH in YSZ–ACAC suspension was used to control the agglomeration of particles and suspension stability. The zeta potential increased with the addition of either organic acid or alkali and enhanced the repulsion between YSZ particles perhaps due to the adsorption of protons and alkali molecules, respectively. The increased electrostatic repulsion reduced the particle coagulation and stabilized the suspension. The suspension properties at different pH were explained by estimating the electrostatic interactions between particles. The lesser degree of particle agglomeration leads to denser packing of particles after EPD and drying. The subsequent sintering also benefited from the higher green density. The moderate agglomeration at pH 4.4 and 8.4 gave a more uniform microstructure and better sinterability. The loose particle packing in coatings made at pH 7.4 caused large voids to remain between particle networks after sintering. Accordingly, it is suggested that the microstructure of EPD coatings can be tailored by modifying particle agglomeration via pH adjustment.

Acknowledgements

The authors wish to acknowledge financial support from the Technology Strategy Board and MEL Chemicals for supplying YSZ powder.

References

[1]. Boccaccini, A. and Zhitomirsky, I., Application of electrophoretic and electrolytic deposition techniques in ceramics processing. *Curr. Opin. Solid State Mater. Sci.*, 2002, **6**(3), 251–260.

[2]. Chen, C., Chen, S. and Liu, D., Electrophoretic deposition forming of porous alumina membranes. *Acta Mater.*, 1999, **47**(9), 2717–2726.

[3]. Van der Biest, O., Joos, E., Vleugels, J. and Baufeld, B., Electrophoretic deposition of zirconia layers for thermal barrier coatings. *J. Mater. Sci.*, 2006, **41**(24), 8086–8092.

[4]. Horn, R., Surface forces and their action in ceramic materials. *J. Am. Ceram. Soc.*, 1990, **73**(5), 1117–1135.

[5]. Bleier, A. and Westmoreland, C., Effects of pH and particle-size on the processing of and the development of microstructure in alumina–zirconia composites. *J. Am. Ceram. Soc.*, 1991, **74**(12), 3100–3111.

[6]. Zhitomirsky, I., Cathodic electrodeposition of ceramic and organoceramic materials. Fundamental aspects. *Adv. Colloid Interf. Sci.*, 2002, **97**(1–3), 279–317.

[7]. Reed, J. S., *Principles of Ceramics Processing* (*2nd Edition*). John Wiley and Sons, New York, 1995, pp. 26–27, 163 and 171.

[8]. Bonnas, S., Tabellion, J. and Hausselt, J., Effect of particle size distribution and sedimentation behaviour on electrophoretic deposition of ceramic suspensions. *Electroph. Depos. Fund. Appl. II, Key Eng. Mater.*, 2006, **314**, 69–74.

[9]. Lewis, J., Colloidal processing of ceramics. *J. Am. Ceram. Soc.*, 2000, **83**(10), 2341–2359.

[10]. Wang, G., Sarkar, P. and Nicholson, P., Influence of acidity on the electrostatic stability of alumina suspensions in ethanol. *J. Am. Ceram. Soc.*, 1997, **80**(4), 965–972.

[11]. Widegren, J. and Bergstrom, L., The effect of acids and bases on the dispersion and stabilization of ceramic particles in ethanol. *J. Eur. Ceram. Soc.*, 2000, **20**(6), 659–665.

[12]. Ma, J. and Cheng, W., Deposition and packing study of sub-micron PZT ceramics using electrophoretic deposition. *Mater. Lett.*, 2002, **56**(5), 721–727.

[13]. Zhang, J. and Lee, B., Electrophoretic deposition and characterization of micrometer-scale $BaTiO_3$ based X7R dielectric thick films. *J. Am. Ceram. Soc.*, 2000, **83**(10), 2417–2422.

[14]. Siffert, B., Jada, A. and Eleli-Letsango, J., Stability calculations of TiO_2 nonaqueous suspensions—thickness of the electrical double-layer. *J. Colloid Interf. Sci.*, 1994, **167**(2), 281–286.

[15]. Siffert, B., Jada, A. and Letsango, J., Location of the shear plane in the electric double-layer in an organic medium. *J. Colloid Interf. Sci.*, 1994, **163**(2), 327–333.

[16]. Kallay, N. and Zalac, S., Charged surfaces and interfacial ions. *J. Colloid Interf. Sci.*, 2000, **230**(1), 1–11.

[17]. Sarkar, P. and Nicholson, P., Electrophoretic deposition (EPD): mechanisms, kinetics, and application to ceramics. *J. Am. Ceram. Soc.*, 1996, **79**(8), 1987–2002.

[18]. Anne, G., Neirinek, B., Vanmeensel, K., Van der Biest, O. and Vleugels, J., Origin of the potential drop over the deposit during electrophoretic deposition. *J. Am. Ceram. Soc.*, 2006, **89**(3), 823–828.

[19]. Fukada, Y., Nagarajan, N., Mekky, W., Bao, Y., Kim, H. and Nicholson, P., Electrophoretic deposition—mechanisms, myths and materials. *J. Mater. Sci.*, 2004, **39**(3), 787–801.

[20]. Ma, J., Zhang, R., Liang, C. and Weng, L., Colloidal characterization and electrophoretic deposition of PZT. *Mater. Lett.*, 2003, **57**(30), 4648–4654.

[21]. Tabellion, J. and Clasen, R., Electrophoretic deposition from aqueous suspensions for near-shape manufacturing of advanced ceramics and glasses—applications. *J. Mater. Sci.*, 2004, **39**(3), 803–811.

[22]. Santillan, M., Membrives, F., Quaranta, N. and Boccaccini, A., Characterization of TiO_2 nanoparticle suspensions for electrophoretic deposition. *J. Nanopart. Res.*, 2008, **10**(5), 787–793.

[23]. Rhodes, W., Agglomerate and particle-size effects on sintering yttria-stabilized zirconia. *J. Am. Ceram. Soc.*, 1981, **64**(1), 19–22.

[24]. Rieth, P. and Reed, J., Flexural strength of ultrafine yttria stabilized zirconia. *Am. Ceram. Soc. Bull.*, 1974, **53**(4), 313–1313.

[25]. Bates, R. G., *Determination of pH-theory and practice* (*2nd Edition*). John Wiley and Sons, 1973, pp. 212–242.

[26]. Zhao, X. and Xiao, P., Focus effect of photoluminescence piezospectroscopy and its influence on the stress measurement of thermally grown oxide in thermal barrier coatings. *Scripta Mater.*, 2007, **57**(8), 683–686.

[27]. Risbud, S., Shan, C., Mukherjee, A., Kim, M., Bow, J. and Holl, R., Retention of nanostructure in aluminum-oxide by very rapid sintering at 1150 °C. *J. Mater. Res.*, 1995, **10**(2), 237–239.

[28]. Ji, C., Lan, W. and Xiao, P., Fabrication of yttria-stabilized zirconia coatings using electrophoretic deposition: packing mechanism during deposition. *J. Am. Ceram. Soc.*, 2008, **91**(4), 1102–1109.

[29]. Yuan, Y., Wang, X. and Xiao, P., Attrition milling of metallic-ceramic particles in acetylacetone. *J. Eur. Ceram. Soc.*, 2004, **24**(8), 2233–2240.

[30]. Hunter, R. J., *Foundations of Colloid Science* (*2nd Edition*). Oxford University Press, 2001, pp. 599.

[31]. Ishikawa, Y., Katoh, Y. and Ohshima, H., Colloidal stability of aqueous polymeric dispersions: effect of pH and salt concentration. *Colloids Surf. B*, 2005, **42**(1), 53–58.

[32]. Lide, D. R., *CRC Handbook of Chemistry and Physics* (86th Edition). Taylor and Francis, 2005.

[33]. Van der Hoeven, P. and Lyklema, J., Electrostatic stabilization in nonaqueous media. *Adv. Colloid Interf. Sci.*, 1992, **42**, 205–277.

[34]. Nychka, J., Winter, M., Clarke, D., Naganuma, T. and Kagawa, Y., Temperature-dependent optical reflectivity of tetragonal-prime yttria-stabilized zirconia. *J. Am. Ceram. Soc.*, 2006, **89**(3), 908–913.

[35]. Kellett, B. and Lange, F., Thermodynamics of densification: 1. Sintering of simple particle arrays, equilibrium-configurations, pore stability, and shrinkage. *J. Am. Ceram. Soc.*, 1989, **72**(5), 725–734.